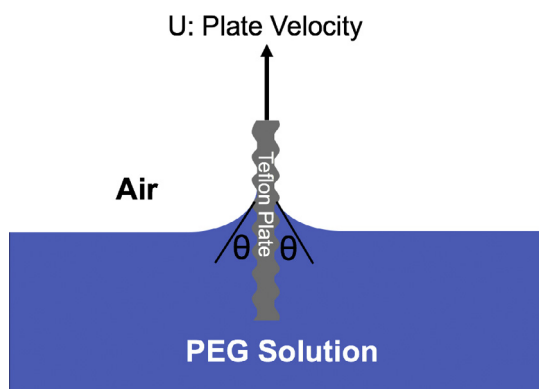


Regular Article

Experimental study of dynamic contact angles on rough hydrophobic surfaces

Alireza Mohammad Karim^{a,*}, Jonathan P. Rothstein^b, H. Pirouz Kavehpour^a^a Department of Mechanical and Aerospace Engineering, UCLA, Los Angeles, CA 90025, USA^b Department of Mechanical and Industrial Engineering, UMass Amherst, Amherst, MA 01003, USA

GRAPHICAL ABSTRACT



ARTICLE INFO

Article history:

Received 6 June 2017

Revised 23 November 2017

Accepted 26 November 2017

Available online 2 December 2017

Keywords:

Dynamic contact angle

Contact line velocity

Rough Teflon plate

Molecular-kinetic theory

Wilhelmy plate method

ABSTRACT

Rough hydrophobic surfaces have many applications in industry and technology. An experimental study was done on the spreading dynamics of different concentrations of polyethylene glycol (PEG) solutions on rough Teflon plates with different roughness. The experiments were conducted using Wilhelmy plate method. The advancing dynamic contact angle was found to be weakly dependent of capillary number. However, the receding dynamic contact angle decreases with increasing capillary number. The degree of roughness on rough Teflon surface has an important role on dynamic contact angle. The dynamics of receding motion was found to follow the molecular-kinetic theory. A power law relation between the receding dynamic contact angle and the capillary number was also obtained.

© 2017 Elsevier Inc. All rights reserved.

1. Introduction

There is some degree of roughness on most of practical solid surfaces. There were many studies about spontaneous spreading of liquid droplets on rough hydrophilic surfaces [1–4]. Controlling

the wettability (i.e. spreading of water or an aqueous solution) on rough hydrophobic surfaces is very important in industry such as coating, ink-jet printing, waterproof clothing, power plants, airplane wings, micro-channels, and satellite communication devices, etc. [5–19].

There are two important factors to control the wettability: the chemical composition of the surface and the degree of surface roughness [11]. Roughness increase on a hydrophobic surface,

* Corresponding author.

E-mail address: amohamma@umn.edu (A. Mohammad Karim).

increases the hydrophobicity because of incorporating air on the solid surface. Air pockets form within the peaks of the surface roughness which leads to the presence of the combined partial liquid-air interface and the partial solid-liquid interface. This is known as Cassie-Baxter state of the equilibrium contact angle. In a Cassie-Baxter state, both the equilibrium advancing and receding contact angles are very large resulting an almost negligible contact angle hysteresis. Alternatively, creating surface roughness on a hydrophobic surface, over which no air pocket exists, forms larger solid-liquid interface. That results a higher apparent contact angle due to the increase in the hydrophobic surface. This is known as Wenzel state of the equilibrium contact angle.

Recently, Kim and Rothstein performed an experimental study on spreading dynamics on hydrophobic and super-hydrophobic surfaces [20]. They prepared a systematically patterned super-hydrophobic surfaces by hot embossing a pattern of micro-posts into a smooth Teflon surface [20]. Their super-hydrophobic surfaces exhibited the Cassie-Baxter state [20]. They have measured advancing and receding dynamic contact angles at different contact line velocity and capillary number using the optical method. They found that the advancing contact angle is independent of capillary number and contact line velocity. They observed that the receding contact angle decreases with increase in capillary number. However, they reported a much weaker dependence of the receding contact angle on capillary number for the super-hydrophobic surfaces.

So far, there has not been any experimental study on the spreading dynamics on rough hydrophobic surfaces with the Wenzel state of the equilibrium contact angle. Here, we experimentally study on the dynamic contact angle on rough hydrophobic surfaces with the Wenzel state of the equilibrium contact angle.

There are two general approaches to describe the dependency of the dynamic contact angle on the speed of the liquid contact line: the hydrodynamics and the molecular-kinetic approach [21].

Hydrodynamics theory (HDT) determines the relation between the dynamic contact angle and the velocity of the liquid contact line by focusing on the bulk motion of liquid on the solid surface. Hydrodynamic theory considers the viscous dissipation due to the flow of liquid on the solid substrate by applying the lubrication approximation on the Navier-Stokes equations [22–30]. As a result, Eq. (1) shows the dependency of the dynamic contact angle to the liquid contact line velocity using HDT.

$$\theta^3 - \theta_0^3 = \pm \frac{9\mu U}{\sigma} \ln\left(\frac{L}{L_s}\right) \quad (1)$$

In Eq. (1), the plus and minus signs are for the advancing and receding motion of the liquid contact line, respectively. In Eq. (1), θ is the dynamic contact angle, θ_0 is the equilibrium contact angle, μ is the dynamic viscosity, σ is the surface tension, U is the liquid contact line velocity, L is the characteristic length of flow, and L_s is the slip length over which the slip condition happens at the solid/liquid interface.

Molecular-kinetic theory (MKT) describes the dependency of the dynamic contact angle to the liquid contact line velocity based on the molecular displacements of liquid molecules on the solid surface at the vicinity of the liquid contact line by considering both solid and liquid properties [31,32]. Blake [31,32] applied the absolute activated reaction rate theory proposed by Glasstone, Laidler, and Eyring [33] to describe this relation as shown in Eq. (2):

$$\theta = \cos^{-1} \left(\cos \theta_0 \pm \frac{2k_B T}{\sigma \lambda^2} \sinh^{-1} \left(\frac{U}{2K_w \lambda} \right) \right) \quad (2)$$

In Eq. (2), the minus sign and plus sign refer to the advancing motion and the receding of the liquid contact line, respectively. In Eq. (2), θ is the dynamic contact angle, θ_0 is the equilibrium con-

tact angle, k_B is the Boltzmann constant, T is the temperature, σ is the surface tension, and U is the liquid contact line speed. λ is defined as the average molecular distance between two adjacent adsorption sites (i.e. sites where liquid molecules attach/detach on/from the solid surface) on the solid surface or average molecular displacement at the vicinity of the liquid contact line. K_w is defined as the frequency of molecular attachment/detachment at equilibrium state.

2. Experimental section

2.1. Materials

The solid substrates used in this experimental study were rough Teflon plates. They were prepared by placing smooth Teflon plates in between two wire meshes of corrosion-resistant-stainless-steel-wire-cloth with the mesh size of interest. The mesh sandwiched Teflon plate was placed between two aluminum plates and pressed with a mechanical press by applying large compressive force with the manual presser (Fig. 1). Then the compressed sandwiched Teflon plate was placed inside an oven. The oven was set to heat up the sandwiched Teflon plate at a temperature of 149 °C for almost 2.5 h. Then the oven was turned off and waited for the oven to cool off for a day. The posts (i.e. bumps) were formed on the smooth Teflon surface by the stainless-steel wire mesh. The uniform roughness (i.e. uniform posts) was patterned evenly on both sides of the Teflon plate. The experiments were performed on the uniform rough Teflon plates. The experiments were done for three rough Teflon plates with three different degrees of roughness. The images of the rough Teflon plates prepared for the experiments are shown in Fig. 2.

The geometric specifications of the corrosion-resistant stainless steel woven wire cloths with three mesh sizes (i.e. 40 × 40 mesh size, 200 × 200 mesh size, and 400 × 400 mesh size) are shown in Table 1.

The liquids used in this study were solutions of polyethylene glycol (PEG) mixed with pure water in two different weight ratios. Both solutions have almost the same surface tension but with different dynamic viscosities. The dynamic viscosities were measured using a stress-controlled rheometer. Both solutions exhibited the Newtonian behavior. The surface tensions were measured using the ring tear-off method with tensiometer (K100 Krüss). The densities were also measured experimentally using the tensiometer (K100 Krüss). The physical properties (i.e. the densities, the dynamic viscosities, and the surface tensions) are given in Table 2.

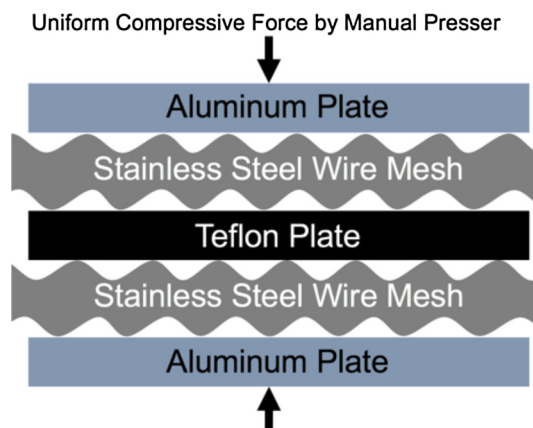


Fig. 1. The schematics to illustrate embossing the Teflon plate with stainless steel wire meshes.

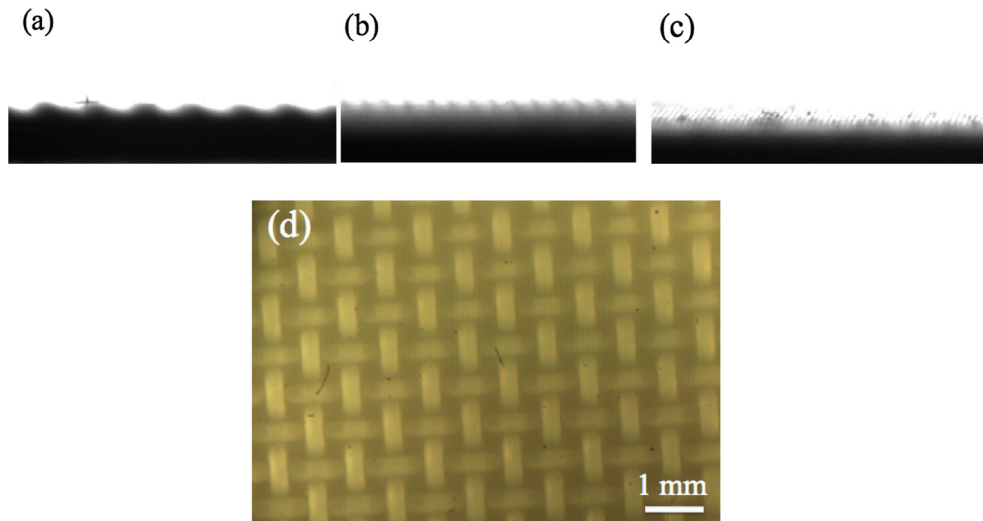


Fig. 2. The side view images of rough Teflon plates patterned with mesh size that were taken with camera used in drop shape analyzer (DSA) for (a) 40×40 , (b) 200×200 , and (c) 400×400 . (d) The microscopic image of the top view of rough Teflon plate for 40×40 .

Table 1

The geometric specifications of corrosion-resistant type 304 stainless steel woven wire cloth for three different mesh sizes. a: opening size, size of roughness (posts), b: wire diameter, height of roughness and distance between roughness.

Mesh size	a [m]	Open Area [%]	b [m]
40×40	30.5×10^{-5}	21	34.3×10^{-5}
200×200	8.6×10^{-5}	46	4.1×10^{-5}
400×400	3.8×10^{-5}	36	2.5×10^{-5}

Table 2

The measured physical properties of the PEG solutions used in the experiments with tensiometer. ρ : density. μ : dynamic viscosity. σ : surface tension.

PEG [%]	ρ [kg/m ³]	μ [Pa s]	σ [N/m]
10	1012	0.06	0.053
20	1031	0.13	0.051

2.2. Experimental set-up

The tensiometer (K100 Krüss) was used to conduct the experiments for forced spreading of PEG solutions on rough Teflon plates. Fig. 3a shows the schematic picture of a tensiometer during the motion of plate in the liquid.

The tensiometer applies the force balance method (i.e. Wilhelmy plate method) to measure the advancing and receding

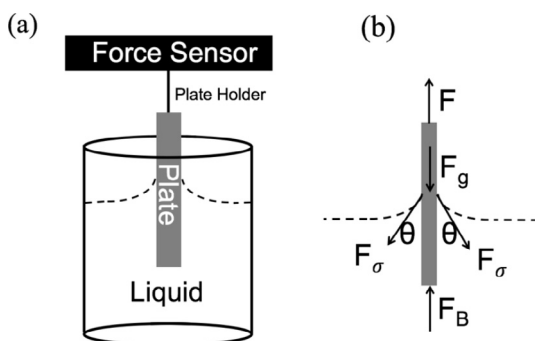


Fig. 3. (a) Schematic of tensiometer. (b) Free-body diagram of forces applied on the plate during its motion in a liquid pool.

dynamic contact angles at the liquid contact line during the advancing and receding motion of the rough Teflon plate in the pool of liquid, respectively. The measurements of the dynamic contact angles were done for three cycles of motion for each set of experiments. A force sensor measured the force applied on the plate of solid substrate and then the tensiometer software calculated the advancing and receding dynamic contact angles using the equation of force balance applied on the plate based on the free-body diagram shown in Fig. 3b during the advancing and the receding motion for each cycle. The velocity of motion of the sample platform, which holds the container, is set to a constant value to maintain a steady-state motion of the liquid contact line during the advancing and the receding motion of plate in the pool of liquid.

The forces applied on the plate during its motion are gravitational force, F_g , due to the weight of the plate, force from the plate holder on the plate being measured by the force sensor, F , capillary force, F_σ , due to the surface tension of the liquid, and the buoyancy force, F_B , due to the difference between the density of plate, ρ_{plate} , and the density of liquid, ρ .

$$F_\sigma = 2\sigma(w + t) \cos \theta \quad (3)$$

$$F_B = \rho g w t x \quad (4)$$

$$F_g = \rho_s g w t L \quad (5)$$

In Eqs. (3)–(5), L is the length of the plate, w is the width of the plate, t is the thickness of the plate, σ is the surface tension of the liquid, ρ is the density of the liquid, ρ_s is the density of the plate, g is gravitational acceleration, θ is the dynamic contact angle, and x is the immersion depth. As a result, Eq. (6) shows the force balance for the steady-state motion of the plate in the liquid as follows:

$$F - F_\sigma + F_B - F_g = 0 \quad (6)$$

The gravitational force is calibrated at the onset of contact of the plate with the liquid. Hence, Eq. (7) expresses the balance of forces applied on the plate for maintaining constant speed of the liquid contact line during the advancing and the receding motion by excluding the effect of the gravitational force during the experiment for each cycle.

$$F - F_\sigma + F_B = 0 \quad (7)$$

By substituting Eqs. (3) and (4) into Eq. (7), using the values of experimentally measured applied force on the plate from the force sensor for F , knowing the physical properties of the liquid, and the geometric specifications of the solid plate, the contact angle can be calculated from Eq. (7).

3. Results and discussion

Forced spreading experiments were performed for two PEG solutions on three rough Teflon plates. The experiments were done using a tensiometer with three cycles of advancing and receding motions. Besides to the viscosity of the PEG solution, the only parameter that changes from one experiment to the next is the velocity of immersion (i.e. advancing motion) and the velocity of emersion (i.e. receding motion) for each specific Teflon/PEG solution system. Fig. 4 shows the advancing dynamic contact angle, θ_A , versus the capillary number ($Ca = \frac{\mu U}{\sigma}$) for 10 wt% and 20 wt% PEG solutions on rough Teflon plates with roughness densities (40×40 , 200×200 , and 400×400). The results show a weak dependence of the advancing dynamic contact angle on capillary number unlike the case for smooth Teflon surface [34] (Fig. 4). The advancing dynamic contact angle is linearly weakly dependent of capillary number within the range of the capillary numbers tested for the case of forced spreading of 20 wt% PEG solution on rough hydrophobic surfaces (Fig. 4). However, in the case of forced spreading of 10 wt% PEG solution on rough hydrophobic surfaces, almost no dependency of advancing dynamic contact angle on capillary number was observed, but perhaps that is just because of the low capillary number region unless weakly dependence may have been able to be observed. Low capillary number is associated with small contact line velocities at which the experiments were conducted and the low shear viscosity of 10 wt% PEG solution. Both substantially reduce the viscous effect on liquid spreading and hence eliminating the dependency of advancing dynamic contact angle on capillary number. The independence of the advancing dynamic contact angle on capillary number has been observed by Rothstein and his co-workers for forced spreading on rough hydrophobic surfaces in the Cassie-Baxter state [20]. The independence or weakly dependence of advancing dynamic contact angle on capillary number is related to the presence of the roughness

on a hydrophobic surface. This could be because the rough hydrophobic surface saturates at high advancing contact angles and begins to entrain air. At large advancing dynamic contact angles, the liquid contact line lies well below the liquid bulk placed on the moving rough hydrophobic surface, which causes the presence of slip of the liquid contact line along the posts on the rough hydrophobic surface. This can lead to the entrainment of air between the liquid and the posts of the rough hydrophobic surface. That is speculative, but it has been observed for spreading on smooth surface at high capillary numbers. The reliefs of the surface morphology of rough Teflon plates can also be referred to as posts. The advancing contact angle increases with decreasing post size (Fig. 4). This should be related to the energy of contact line pinning, which goes down per post, as the posts get smaller even if the total contact line pinning energy stays the same per unit length. This means that as the liquid contact line moves from a post to the next on a rough hydrophobic surface roughened with small posts, the liquid contact line seems to be more in contact with air than solid surface. This may be the reason that the liquid contact line can move easily on the rough hydrophobic surface roughened with small posts [35].

Fig. 5 shows the receding dynamic contact angle, θ_R , versus capillary number for PEG solutions on rough Teflon plates. The results show significant dependence of the receding dynamic contact angle on capillary number like the case for smooth Teflon surface [34] (Fig. 5). In these experiments, the equilibrium contact angle is at the Wenzel state, hence the liquid contact line is in contact with all surface area of the posts. As the heights of the posts increase, the receding dynamic contact angle increases for the same PEG solution on a given liquid contact line velocity except for the case of smooth Teflon plates (Fig. 5). This is related to the fact that in the Wenzel state all surface area of the posts is wetted. The receding dynamic contact angle increases as viscosity increases for the experiments on the same Teflon surface except for the case of 305 μm mesh-size Teflon plates. The 20 wt% PEG solutions on 86 μm and 305 μm mesh-size Teflon plates have similar receding contact angles, especially for low Ca . This may be associated with the fact that for large posts (86 μm and 305 μm) and at small capillary numbers, the pinning effect becomes independent of the post's size. This may cause similar receding

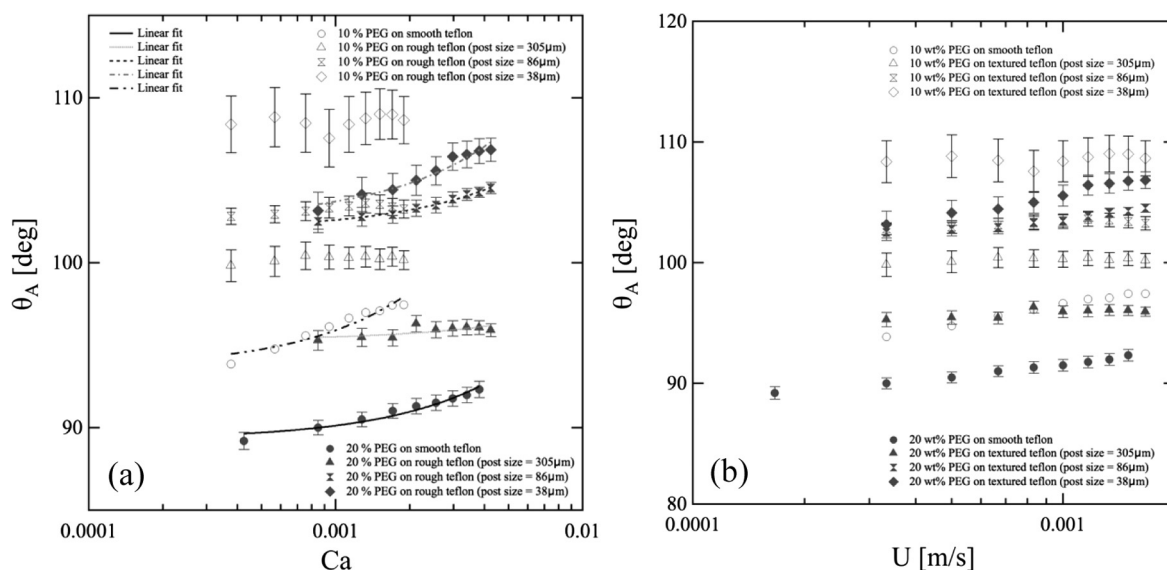


Fig. 4. Advancing motion of PEG/water mixtures versus (a) capillary number and (b) contact line speed. The error bar shown for the data designates the range of the data for the 3 runs conducted at each capillary number or contact line speed.

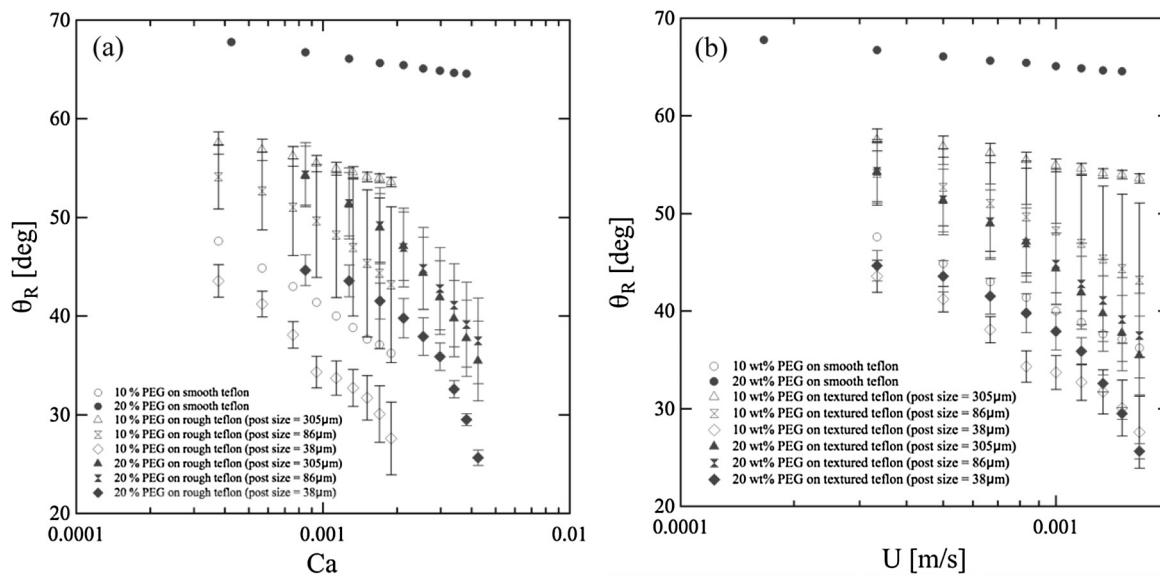


Fig. 5. Receding motion of PEG/water mixtures versus (a) capillary number and (b) contact line speed. The error bar shown for the data designates the range of the data for the 3 runs conducted at each capillary number or contact line speed.

dynamic contact angles for each Ca . All the other samples show significantly different results at all Ca tested in the experiments.

Fig. 6 shows the contact angle hysteresis (i.e. difference between the advancing and the receding contact angle) versus capillary number. As capillary number increases, the contact angle hysteresis increases. Area fraction of posts on the surface is the same. The number of posts formed per unit surface area of the flat Teflon surface is the only parameter that effects on the true area of the rough hydrophobic surface in contact with the liquid contact line. As the post-size decreases, the number of posts formed per unit surface area of the flat Teflon surface increases. As the number of posts per unit surface area of the flat Teflon surface increases, the surface area in contact with the liquid contact line increases. Hence the liquid contact line has less contact with air and more contact with the solid surface. This can lead to increase the pinning effect along the edges of the posts, which causes a larger pinning force leading to a larger contact angle hysteresis for each liquid

contact line velocity (Fig. 6). The changes in the number of the posts on the rough surfaces has no influence on the slope of variation of the contact angle hysteresis versus capillary number.

The relation between the receding dynamic contact angle and liquid contact line velocity were analyzed by applying HDT and MKT. The only free fitting parameter for analysis with HDT is the slip length, L_s . The slip length value must be in the order of microns. The free fitting parameters for analysis with MKT are K_w and λ . In fitting analysis, we impose the constraints on range of values λ can physically vary, which is in order of nanometers. The MKT was the best appropriate model to describe the dependency of the receding dynamic contact angle on range of capillary number tested in the experiments (Fig. 7). As it was noted in the introduction, MKT explains the liquid contact line dynamics (i.e. dependency of dynamic contact angle to contact line velocity) by considering the molecular-scale of adsorption/desorption phenomena at the liquid contact line and its relation to the liquid contact line friction. The liquid contact line friction plays an important role in determining the dynamic contact angles on the rough hydrophobic surfaces due to the pinning effect during the motion of the liquid contact line across the posts on the rough hydrophobic surfaces. Hence MKT is physically the most appropriate model to describe the dynamics of spreading on the rough hydrophobic surfaces. The values of fitting parameters have been summarized Tables 3 and 4.

Figure 8 shows the effect of the geometric specifications of the micron-scale posts on the liquid contact line dynamics (i.e. described by the MKT fitting parameter used in the analysis known as λ) of the PEG solutions on the rough hydrophobic surfaces. a/b ratio shows the non-dimensional geometric property of the micron-scale posts on the rough hydrophobic surfaces used in this study. λ values, obtained from fitting analyses, depend on the size of roughness and the distance between them (Fig. 8). The molecular-displacement, λ , shows a stronger dependency on the dynamic viscosity of liquid (Fig. 8). This signifies that the increase in the dynamic viscosity of the liquid makes the resisting force between the liquid molecules larger hence lowering the average displacement of the liquid molecules near the liquid contact line.

Fig. 9 shows the dependency of $(\theta_{OR}^3 - \theta_R^3)$ on capillary number. The dependence of $(\theta_{OR}^3 - \theta_R^3)$ on the capillary number follows the power law (Eq. (8)):

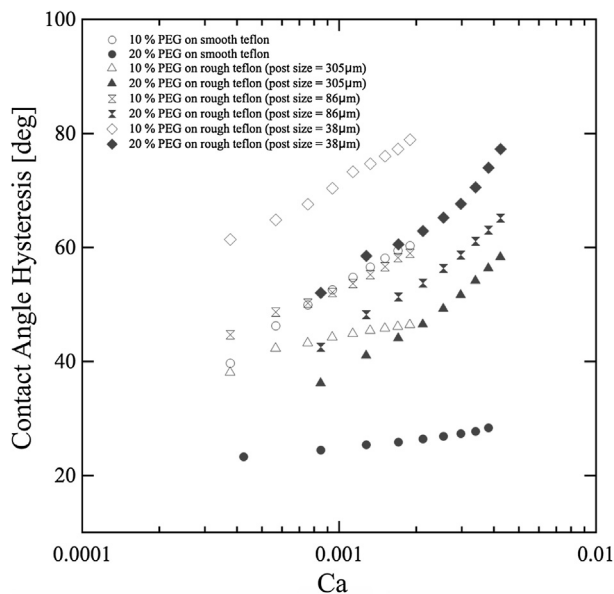


Fig. 6. Contact angle hysteresis versus capillary number for PEG/water mixtures.

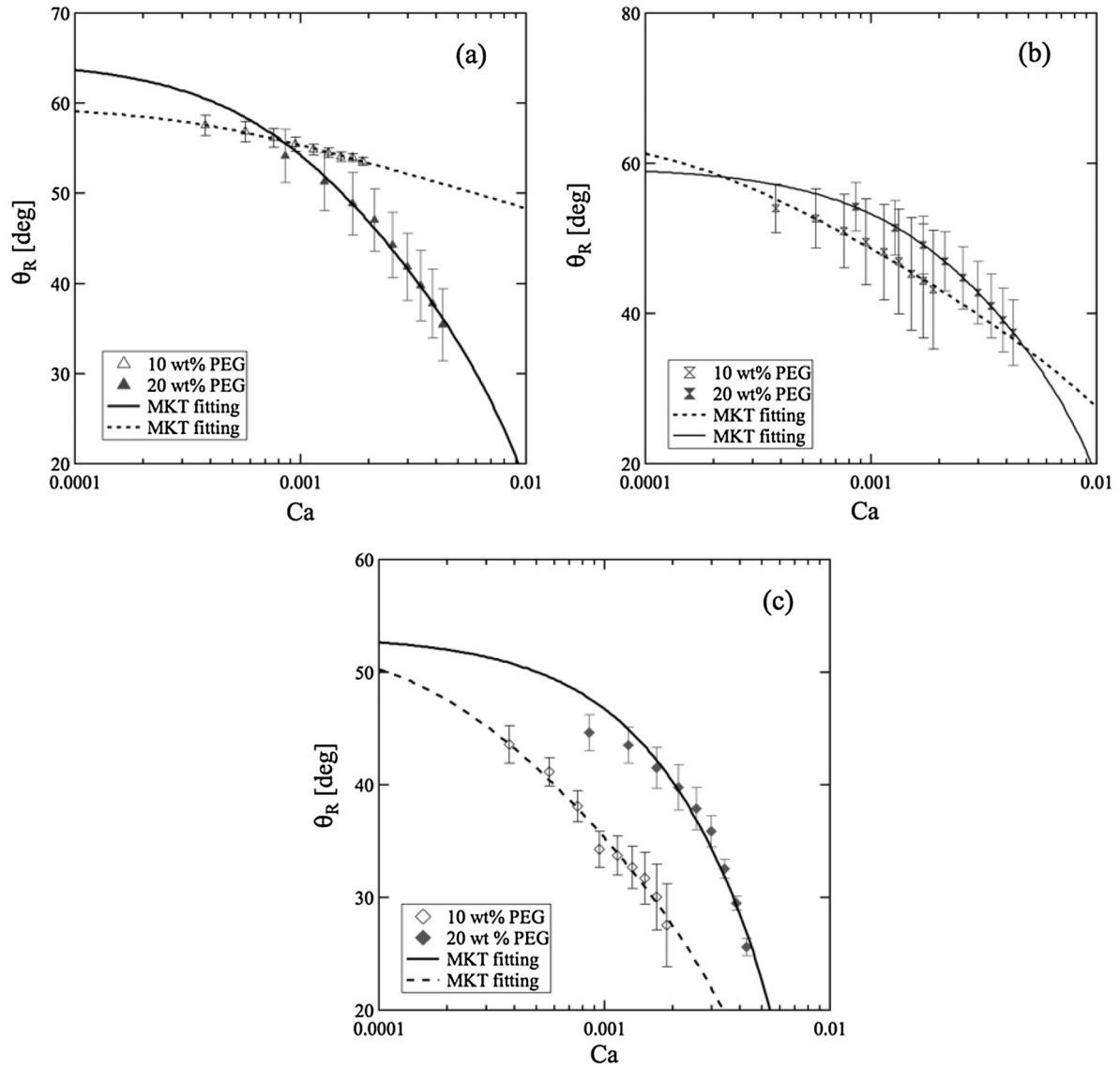


Fig. 7. Receding motion of PEG/water mixtures on rough Teflon plates patterned with mesh size of (a) 40 × 40, (b) 200 × 200, and (c) 400 × 400.

Table 3

The MKT parameters obtained from fitting analysis for forced receding motion on three rough Teflon surfaces for the case of 10 wt% PEG/water mixture.

Rough surface post size	λ [nm]	K_w [kHz]	θ_0 [deg]
305	1.9 ± 0.1	110 ± 40	59.7 ± 0.5
86	1.3 ± 0.1	71 ± 49	64.4 ± 2.9
38	1.23 ± 0.04	87 ± 17	53.3 ± 0.0

Table 4

The MKT parameters obtained from fitting analysis for forced receding motion on three rough Teflon surfaces for the case of 20 wt% PEG/water mixture.

Rough surface post size	λ [nm]	K_w	θ_0 [deg]
305	0.97 ± 0.04	190 ± 70	64.9 ± 1.7
86	0.92 ± 0.01	430 ± 40	59.6 ± 0.3
38	0.84 ± 0.18	580 ± 550	53.3 ± 0.0

$$(\theta_{OR}^3 - \theta_R^3) \sim Ca^n \tag{8}$$

The existence of liquid/air contact surface occurring along the rough Teflon surfaces during the forced receding may cause the power law (Eq. (8)) with $n \neq 1$ for the case of Wenzel state for large

capillary numbers. For capillary numbers less than 0.001, the results show Eq. (8) with $n = 1$. Power laws with lower powers (e.g. 1/3) have been obtained by Rothstein and his co-workers based on the optical technique [20] for the case of Cassie-Baxter state.

4. Summary and conclusions

PEG is used as a lubricating coating in industry for various surfaces due to its low toxicity and high flexibility and perfect water-solubility [36]. Teflon is extensively used in aerospace and computer industry due to its excellent insulating and naturally hydrophobic properties. Teflon's low coefficient of friction with many surfaces and its 'non-stick' properties are perfect material candidate for cookware [37]. Experimental study of the dynamic contact angles of PEG solutions on rough Teflon plates were performed using tensiometer. To avoid the influence of viscous drag on tensiometer calculation of dynamic contact angles, low concentrations of PEG were used to prepare the PEG solutions for the experiments. The main purpose to choose the types of roughness used in this experimental was only to show the fundamental effect of posts' size on the spreading dynamics especially in micron-scale.

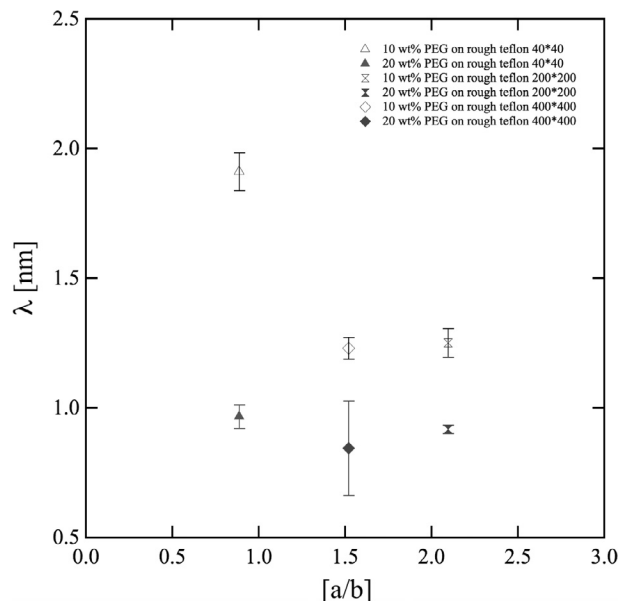


Fig. 8. Plot of λ , average molecular-displacement at the liquid contact line, versus $[a/b]$, roughness (post) size over distance between roughness (posts).

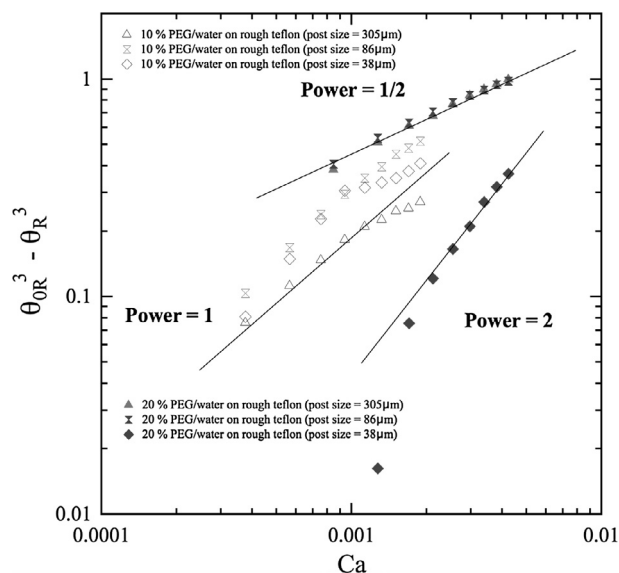


Fig. 9. Alternative form of describing the spreading dynamics for receding motion of PEG/water mixtures on rough Teflon plates.

The equilibrium contact angles were at Wenzel state ranging from 100° to 120° . Roughness (posts) on smooth Teflon surfaces has an important effect on both advancing and receding dynamic contact angles.

The advancing dynamic contact angle was weakly dependent on the capillary numbers tested as it had been also observed for the Cassie-Baxter [20]. However, in the case of Wenzel state, the advancing dynamic contact angle is weakly dependent on the capillary number unlike the complete independence of advancing dynamic contact angle on capillary number for Cassie-Baxter state [20]. Generally, it can be noted that the effect of roughness (posts) on hydrophobic surface reduces the dependence of the advancing dynamic contact angle on capillary number. This can be related to the pinning force along the rough hydrophobic surface. The advancing contact angle increases with decreasing post size, but

that relation is not very strong. That is related to the decrease of energy of contact line pinning per post as the posts get smaller even if the total contact line pinning energy stays the same per unit length. This means that as the liquid contact line moves from a post to the next on a rough hydrophobic surface roughened with small posts, the liquid contact line seemingly is more in contact with air than solid surface. This may be the reason that the liquid contact line easily moves on the rough hydrophobic surface roughened with small posts.

The receding dynamic contact angle was dependent on capillary number. The increase on the post size on the rough surface causes the value of the receding dynamic contact angle to decrease. The increase of post size on the rough surfaces has no effect on the slope of change of the contact angle hysteresis versus capillary number.

The dependency of the receding dynamic contact angle on the contact line velocity were analyzed using hydrodynamics and molecular-kinetic theory. The hydrodynamics theory was not an appropriate model to describe the relation as has also been concluded by Rothstein and his co-workers [20] for Cassie-Baxter state. This is caused by the effect of pinning and the presence of the partial slip-condition along the rough surface. The molecular-kinetic theory was found to be the appropriate model by considering the molecular level of adsorption/desorption at the liquid contact line and its relationship with the liquid contact line friction and the pinning effect along the edges of the posts. We have also obtained an empirical power law relation between the cube of receding dynamic contact angle and the capillary number with power of one for low capillary number and deviating from a power of one as the capillary number increases. For the case of Cassie-Baxter state of equilibrium contact angle, power law with lower power (1/3) was obtained by Rothstein and his co-workers [20].

Though we obtained power law relations for the receding dynamic contact angle versus capillary number, we expected the results follow the power law with same power. However, this conclusion is not certain and it requires further study for larger capillary numbers which is not feasible with the capability of the tensiometer because of the effect of the viscous drag on the dynamic contact angle measurement beyond certain velocity range. Nevertheless, this experimental study can lead to the further future research in the complications of the forced spreading on rough hydrophobic surfaces.

References

- [1] M. Apel-Paz, A. Marmur, Spreading of liquids on rough surfaces, *Colloid Surf.* 146 (1999) 273–279.
- [2] A.M. Cazabat, M.A.C. Stuart, Dynamics of wetting on smooth and rough surfaces, *Prog. Coll. Pol. Sci.* 74 (1987) 69–75.
- [3] S.J. Kim, J. Kim, M.W. Moon, K.R. Lee, H.Y. Kim, Experimental study of drop spreading on textured superhydrophilic surfaces, *Phys. Fluids* 25 (2013) 092110.
- [4] J.F. Oliver, S.G. Mason, Microspreading studies on rough surfaces by scanning electron microscopy, *J. Colloid. Interf. Sci.* 60 (1977) 480–487.
- [5] Y. Pomeau, J. Vannimenus, Contact angle on heterogeneous surfaces: weak heterogeneities, *J. Colloid Interf. Sci.* 104 (2) (1985) 477–488.
- [6] M.L. Heck, D.V. Papavassiliou, Effects of hydrophobicity-inducing roughness on micro-flows, *Chem. Eng. Commun.* 200 (2013) 919–934.
- [7] K.M. Smyth, A.T. Paxson, H. Kwon, K.K. Varanasi, Visualization of contact line motion on hydrophobic textures, *Surf. Innovat.* 1 (S12) (2013) 84–91.
- [8] A. Lafuma, D. Quere, Superhydrophobic states, *Nat. Mater.* 2 (2003) 457–460.
- [9] B. He, J. Lee, N.A. Patankar, Contact angle hysteresis on rough hydrophobic surfaces, *Colloid Surf.* 248 (2004) 101–104.
- [10] J.F. Joanny, P.G. de Gennes, A model for contact angle hysteresis, *J. Chem. Phys.* 81 (1) (1984) 552–562.
- [11] C. Dorrer, J. Ruhe, Some thoughts on superhydrophobic wetting, *Soft Matter* 5 (2009) 51–61.
- [12] B. Bhushan, Y.C. Jung, Wetting study of patterned surfaces for superhydrophobicity, *Ultramicroscopy* 107 (2007) 1033–1041.
- [13] J. Ou, B. Perot, J.P. Rothstein, Laminar drag reduction in microchannels using ultrahydrophobic surfaces, *Phys. Fluids* 16 (2004) 4635–4643.
- [14] R.J. Daniello, N.E. Waterhouse, J.P. Rothstein, Drag reduction in turbulent flows over superhydrophobic surfaces, *Phys. Fluids* 21 (2009) 085103.

- [15] R.E. Johnson Jr, R.H. Dettre, Contact angle hysteresis. iii. study of an idealized heterogeneous surface, *J. Phys. Chem.* 68 (7) (1964) 1744–1750.
- [16] D. Quere, Non-sticking drops, *Rep. Prog. Phys.* 68 (2005) 2495–2532.
- [17] G. McHale, N.J. Shirtcliffe, M.I. Newton, Super-hydrophobic and super wetting surfaces: analytical potential?, *Analyst* 129 (2004) 284–287.
- [18] M. Callies, D. Quere, On water repellency, *Soft Matter* 1 (2005) 55–61.
- [19] X. Feng, L. Jiang, Design and creation of superwetting/antiwetting surfaces, *Adv. Mater.* 18 (2006) 3063–3078.
- [20] J.H. Kim, H.P. Kavehpour, J.P. Rothstein, Dynamic contact angle measurements on superhydrophobic surfaces, *Phys. Fluids* 27 (2015) 032107.
- [21] A.M. Cazabat, M.A.C. Stuart, Dynamics of wetting: effects of surface roughness, *J. Phys. Chem.-US* 90 (22) (1986) 5845–5849.
- [22] P.G. de Gennes, Wetting: statics and dynamics, *Rev. Mod. Phys.* 57 (3) (1985) 827–863.
- [23] C. Huh, S.G. Mason, The steady movement of a liquid meniscus in a capillary tube, *J. Fluid Mech.* 81 (1977) 401–419.
- [24] E.B. Dussan, S.H. Davis, On the motion of a fluid-fluid interface along a solid surface, *J. Fluid Mech.* 65 (1974) 71–95.
- [25] O.V. Voinov, Hydrodynamics of wetting *Izvestiya Akademii Nauk SSSR, Mekh. Zhid-kosti i Gaza* 5 (1976) 76–84.
- [26] R.G. Cox, The dynamics of the spreading of liquids on a solid surface. part 1. viscous flow, *J. Fluid Mech.* 168 (1986) 169–194.
- [27] P.G. de Gennes, Deposition of langmuir-blodgett layers, *Colloid Polym. Sci.* 264 (1986) 463–465.
- [28] C. Huh, L.E. Scriven, Hydrodynamic model of steady movement of a solid/liquid/fluid contact line, *J. Colloid Interf. Sci.* 35 (1971) 85–101.
- [29] L.H. Tanner, The spreading of silicone oil drops on horizontal surfaces, *J. Phys. D: Appl. Phys.* 12 (9) (1979) 1473–1484.
- [30] L.M. Hocking, A moving fluid interface. part 2. the removal of the force singularity by a slip flow, *J. Fluid Mech.* 79 (1977) 209–229.
- [31] T.D. Blake, J.M. Haynes, Kinetics of liquid/liquid displacement, *J. Colloid Interf. Sci.* 30 (1969) 421–423.
- [32] T.D. Blake, *Dynamic Contact Angles and Wetting Kinetics*, in: J. C. Berg (Ed.), *Wettability*, Marcel Dekker, 1993, pp. 251–309.
- [33] S. Glasstone, K.J. Laidler, H.J. Eyring, *The theory of rate processes*, *Ind. Eng. Chem.* 33 (1941) 430.
- [34] A. MohammadKarim, H.P. Kavehpour, Dynamics of spreading on ultrahydrophobic surfaces, *J. Coat. Technol. Res.* 12 (5) (2015) 959–964.
- [35] D. Oner, T.J. McCarthy, Ultrahydrophobic surfaces. effects of topography length scales on wettability, *Langmuir* 16 (2000) 7777–7782.
- [36] P.C. Nalam, J.N. Clasohm, A. Mashaghi, N.D. Spencer, Macrotribological studies of poly(L-lysine)-graft-Poly(ethylene glycol) in aqueous glycerol mixtures, *Tribol. Lett.* 37 (3) (2009) 541–552.
- [37] M.A. Nilsson, R.J. Daniello, J.P. Rothstein, A novel and inexpensive technique for creating superhydrophobic surfaces using Teflon and sandpaper, *J. Phys. D: Appl. Phys.* 43 (2010) 045301.